

Novel Lithium-Ion Capacitor Based on TiSb_2 as Negative Electrode: The Role of Mass Ratio towards High Energy-to-Power Densities and Long Cyclability

María Arnaiz,^[a, b] Juan L. Gómez-Cámer,^[a] Federico Mijangos,^[b] Teófilo Rojo,^[a, c] Eider Goikolea,^{*[c]} and Jon Ajuria^{*[a]}

In this work lithium ion capacitors (LICs) built using a TiSb_2 alloy as the negative electrode and activated carbon (AC) derived from recycled olive pits biomass as the positive electrode are reported. TiSb_2 shows high capacity (360 mAh g^{-1} at 10 C) and excellent rate capability performance together with exceptional volumetric features, enabling its use as a promising candidate for high power requiring technologies. So far, to the best of our knowledge, this is the first Sb alloy-based LIC ever reported. In order to maximize the output performance, the influence of the mass ratio of the active materials (TiSb_2 :AC) is studied. The best

TiSb_2 -based LIC is able to deliver an energy density as high as $167 \text{ Wh kg}_{\text{AM}}^{-1}$ (78 Wh dm^{-3}) at $115 \text{ W kg}_{\text{AM}}^{-1}$ (53 W dm^{-3}), more than a 6-fold increase with respect to its EDLC counterpart. Under high power demanding situations, *i.e.*, $11 \text{ kW kg}_{\text{AM}}^{-1}$ (6 kW dm^{-3}), it retains up to $90 \text{ Wh kg}_{\text{AM}}^{-1}$ (48 Wh dm^{-3}), which is among the best reported values for LICs. In addition, the device with the most appropriate mass ratio presents an encouraging 80% retention of the initial capacitance after 10000 charge-discharge cycles at $t_{\text{discharge}} = 11 \text{ s}$.

1. Introduction

Research on lithium ion capacitors (LICs) has skyrocketed over the last years in order to cover the energy-power gap existing between electrical double layer capacitors (EDLCs, $<10 \text{ Wh kg}^{-1}$, $>10 \text{ kW kg}^{-1}$) and lithium ion batteries (LIBs, $\sim 200 \text{ Wh kg}^{-1}$, $<1000 \text{ W kg}^{-1}$).^[1–4] LICs are novel next-generation electrical energy storage devices that combine high energy and high power density, as well as safe use and long cycle life features.^[5,6] These promising energy storage systems can cover those applications in which high energy and high power densities are required, such as kinetic energy recovery systems or energy storage in renewable energies.^[7] Reported literature about these lately in fashion devices raised from 12 publications in 2012 to 78 publications in 2017 (source: Web of Science). Not only the raise in publications but also the commercial availability of LICs from companies such as JM energy (2008), Yunasko (2015) or Maxwell (2016)^[8–11] demon-

strates the potential market uptake of this technology. Furthermore, Maxwell Technologies have already delivered the first commercial application of LICs which are being used for rapid energy regeneration in city trams.^[12]

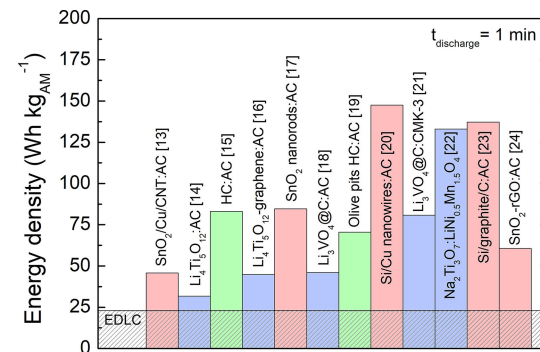


Figure 1. Summary of the energy density values of the latest and more challenging LICs at the discharge time of 1 minute. In red alloy-based LICs, in blue oxide-based LICs and in green carbon-based LICs. The horizontal dashed line represents the gain in energy density in comparison with an EDLC.

Given their bipolar nature, merging the best features of supercapacitors and batteries is key for success. Activated carbon (AC), known by its high specific surface area (SSA) and high conductivity, is the most common material used as capacitor-type material and positive electrode in LICs. Meanwhile, the selection of the battery-type electrode is one of the major challenges of this technology. In Figure 1 some of the latest and more challenging LICs performing at high power demanding conditions, *i.e.*, $t_{\text{discharge}} = 1 \text{ min}$, are summarized.^[13–24]

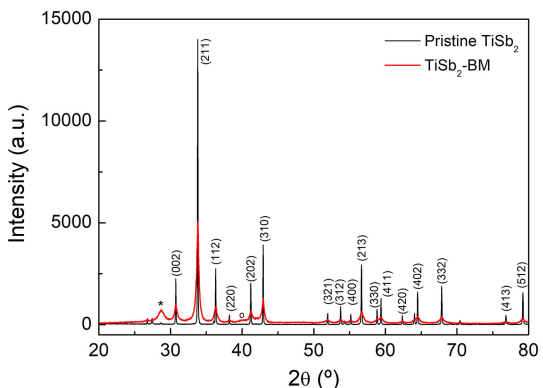
- [a] M. Arnaiz, Dr. J. L. Gómez-Cámer, Prof. T. Rojo, Dr. J. Ajuria
Power Storage, Batteries and Supercaps
CIC energiGUNE
Albert Einstein 48, Technology Park of Alava, 01510 Miñano, Basque Country, Spain
E-mail: jajuria@cicenergigune.com
- [b] M. Arnaiz, Prof. F. Mijangos
Chemical Engineering Department
University of the Basque Country, UPV/EHU
P.O. Box 644, 48080, Leioa, Basque Country, Spain
- [c] Prof. T. Rojo, Dr. E. Goikolea
Inorganic Chemistry Department
University of the Basque Country, UPV/EHU
P.O. Box 644, 48080, Leioa, Basque Country, Spain
E-mail: eider.goikolea@ehu.eus
-  Supporting information for this article is available on the WWW under <https://doi.org/10.1002/batt.201800099>

In this subject, research is focused on the search of new materials that are able to provide not only high energy density but also long cycle life. To achieve this goal, stable materials with good rate capabilities below ~ 1 V vs. Li^+/Li are needed.^[25–27] For that reason, metal alloys studied for LIBs such as Li_xM ($\text{M}=\text{Si}, \text{Sn}, \text{Sb}\dots$) become a good alternative since the potential of many of them is around $\sim 0.3\text{--}1$ V vs. Li^+/Li . Moreover, high specific capacity values of 992 mAh g^{-1} for $\text{Li}_{4.4}\text{Sn}$, 4200 mAh g^{-1} for $\text{Li}_{22}\text{Si}_5$ and 660 mAh g^{-1} for Li_3Sb have been demonstrated.^[27–29] Compared to the specific capacity of graphite (LiC_6 : 372 mAh g^{-1}), they are all excellent alternative candidates to perform as negative electrode. Nevertheless, the large volume changes that these metal alloys suffer results in a large internal stress that weakens their mechanical properties and directly impacts their cycle life. Thus, many efforts are centered on buffering the large volume variations. The main strategies to overcome this problem are focused on reducing the particle size and/or coating the active material with a conductive material such as carbon or graphene,^[30,31] or even with a non-conductive material such as metal oxides.^[32,33] A novel strategy lately in vogue is to synthetize antimony-based intermetallic alloy compounds (MSb_x , where $\text{M}=\text{Ti}, \text{In}, \text{Cu}, \text{Mn}, \text{Co}$ and Zn , and $x=1, 2, 3$) based on an inactive phase that does not react with lithium, and an active phase that it does.^[34–36] The inactive phase allows a fine dispersion of the active element during cycling. This not only avoids the agglomeration of Sb particles and the above mentioned volume changes, but also provides better conductivity to the material and longer cycle life.^[27,32] In this work, the intermetallic compound TiSb_2 , with a specific theoretical capacity of 552 mAh g^{-1} ,^[37] was selected as a potential candidate to substitute graphite as the negative electrode in LICs owing to i) the high specific capacity of Li_3Sb alloy and ii) the lightness of titanium, its non-toxicity and good conductive properties as inactive material.

2. Results and Discussion

In order to confirm the crystalline structure of the synthesized antimony alloy, XRD patterns of the pristine TiSb_2 alloy and the ball milled TiSb_2 ($\text{TiSb}_2\text{-BM}$) are shown in Figure 2. While all the diffraction maxima present in the pristine TiSb_2 can be ascribed to the alloy material,^[38] the ball milled sample shows an additional small peak at 28° and a wide peak at 40° that could be attributed to small amounts of Sb and Ti, respectively, generated during the ball milling process. The broader peaks observed for this last sample suggest an increase in the crystalline planes owing to the particle size reduction. This fact is further confirmed using the Scherrer equation^[39] to calculate the crystalline particle size of each sample, obtaining *ca.* 268 nm size for the pristine sample and *ca.* 16 nm particle size for the ball milled sample.

This is in good agreement with the particle size observed by FE-SEM, where the microstructural analysis certifies a particle size of $\sim 10 \mu\text{m}$ for the pristine alloy (Figure 3a) and about $0.4 \mu\text{m}$ for the ball milled sample (Figure 3b).



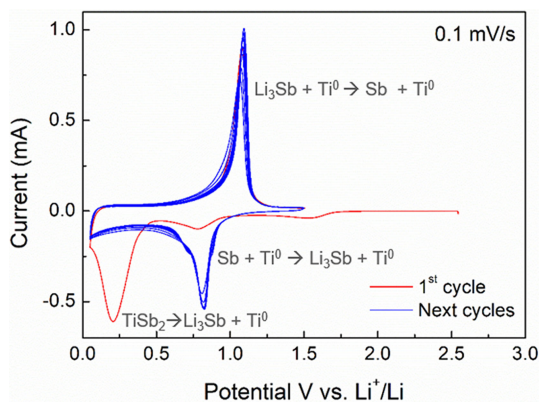


Figure 4. CV of the TiSb₂ alloy between 0.05–1.5 V vs. Li⁺/Li in 1 M LiPF₆ (EC:DMC) at 0.1 mVs⁻¹.

consequence of the lower amount of initial Sb and the less homogeneous particle-size distribution. Moreover, in the case of TiSb₂-BM, around 0.4 V vs. Li⁺/Li, the irreversible reaction from TiSb₂ to Sb occurs (region III). After the first discharge-charge cycle, the plateau at 0.8 V vs. Li⁺/Li is still observed for Sb (Figure 5b) while for TiSb₂-BM a unique sloppy region starting at the same potential, thus, which also corresponds to the alloying reaction, is described. In Figure 5c and 5d, the C-rate capability and stability of both materials are reported. For TiSb₂ the theoretical capacity C is 552 mA g⁻¹ and 660 mA g⁻¹ for Sb.^[27] Initial discharge and charge capacities of TiSb₂ at C/10 are 1140.8 mA h g⁻¹ and 483.3 mA h g⁻¹, respectively, correspond-

ing to a columbic efficiency (CE) of ~42%. This discrepancy between charge and discharge capacities is attributed to the SEI formation and the irreversible conversion reaction from TiSb₂ to Sb. However, TiSb₂ shows excellent reversible capacities in the following cycles onward, with a CE close to 98%. In contrast, owing to the absence of any irreversible conversion reaction, Sb shows a first cycle CE of 71%. At low C-rates both materials deliver a specific capacity as high as 600 mA h g⁻¹. However, in the following cycles, the specific capacity of Sb decreases faster than that of TiSb₂-BM. This rapid capacity fading is attributed to the higher internal mechanical stress caused by the large volume changes undergone by Sb over cycling. The rise of the internal resistance is clearly visible in the Nyquist Plot (Figure S1). In contrast, owing to the titanium matrix, the aforementioned volume expansion and contractions are buffered in TiSb₂-BM and, consequently, it presents high capacity values and an improved capacity retention (see Fig 5d). TiSb₂-BM is capable to store/deliver high specific capacity values such as 463 mA h g⁻¹, 419 mA h g⁻¹, 360 mA h g⁻¹, 264 mA h g⁻¹ and 115 mA h g⁻¹ at 2 C, 5 C, 10 C, 20 C and 50 C respectively. Moreover, as it is shown in Figure S2, the charge/discharge profile features observed at low C-rates remain undistorted even at 20 C ($t_{\text{discharge}} \approx 2$ min). This figure of merit might boost its use as negative electrode for LICs.

LICs assembly was carried out using TiSb₂ as the negative electrode and a previously reported AC derived from olive pits as the positive electrode. They were all assembled in a T-shaped Swagelok® cell using 1 M LiPF₆ (EC:DMC) electrolyte under Ar atmosphere. A key factor for the assembly of a high performing

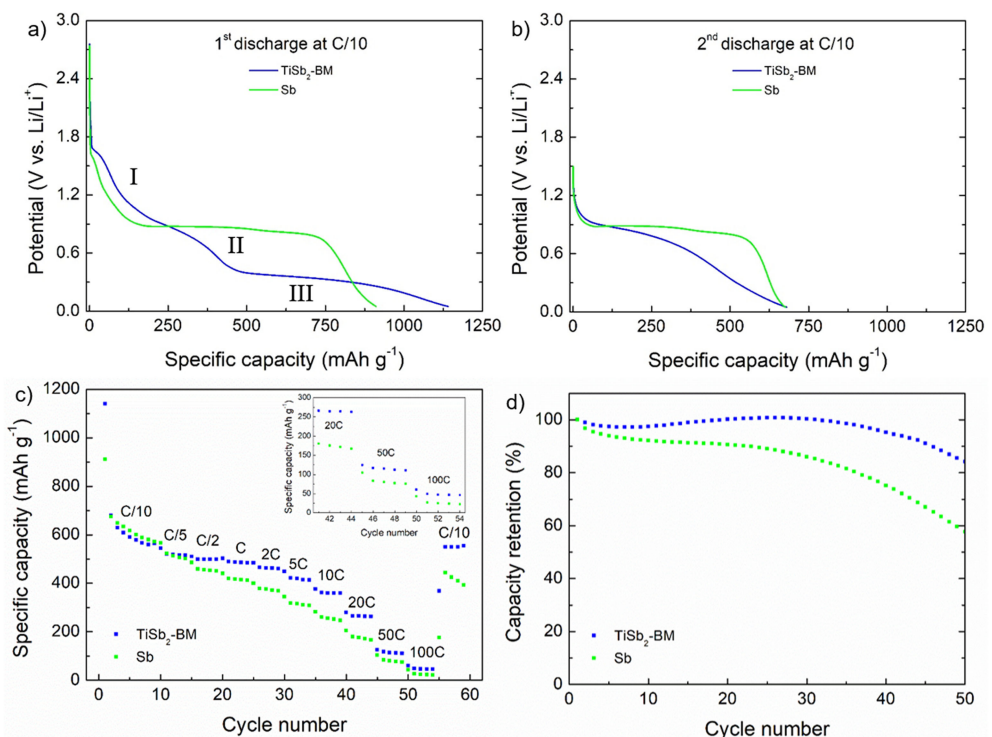


Figure 5. GA charge/discharge measurement for TiSb₂ and Sb between 0.05–1.5 V vs. Li⁺/Li: a) 1st discharge profile at C/10, b) 2nd discharge profile at C/10, c) Rate capability. Inset: zoom of rate capability at high rates and d) Stability test carried out at 5 C.

LIC is an accurate balance of the electrodes in order to maximize the system performance. As the charge stored in both electrodes must be equal ($Q_+ = Q_-$), the mass ratio of active materials ($\text{TiSb}_2:\text{AC}$) must be well balanced to get the maximum capacity output from both materials.^[40] The capacity of both materials diverge differently along the applied current density range and it is not possible to define a suitable mass ratio which could be valid for all the applied range (Figure S3). Thus, a detailed electrochemical study of various $\text{TiSb}_2:\text{AC}$ mass ratios was carried out in order to find out the best combination. In view of the experimental specific capacities of the electrode materials, 1:1, 1:2 and 1:3 mass ratios were selected, herein denoted as LIC (1:1), LIC (1:2) and LIC (1:3).

In order to maximize the output voltage of all studied LICs, both electrodes were preconditioned (Figure S4). TiSb_2 was cycled 5 times between 0.05 and 1.5 V vs. Li^+/Li at 50 mA g^{-1} in order to form the SEI and supply sufficient lithium to compensate for the first cycle irreversibility and then, a cut-off potential of 0.4 V vs. Li^+/Li was set. For the AC, it was charged to a cut-off potential of 4.2 V vs. Li^+/Li at 10 mA g^{-1} . After the preconditioning step, GA charge/discharge measurements were run for all hybrid supercapacitors between 1–3.6 V vs. Li^+/Li at different current densities between 0.05 and 10 A g^{-1} considering the active mass of both positive and negative electrodes.

Since the capacity of the negative electrode is much higher than that of the positive electrode through all the applied current density range, as a first approach, a conservative LIC

(1:1) was studied first. Figure 6 shows GA charge/discharge profiles of each electrode together with the profile of the full LIC system at different applied current densities. At low current densities, *i.e.*, 0.1 A g^{-1} , within a discharge time of 30 min, the positive electrode swings from 2 to 4 V vs. Li^+/Li showing an ideal symmetric profile indicative of a capacitive storage mechanism. Concurrently, the negative electrode swings in a potential window from 1 to 0.5 V, where the alloying reaction of Li_3Sb occurs during the charge of the LIC and the dealloying reaction to Sb during the discharge of the device. Thus, the charge storage of the LIC results from both non-faradic and faradic mechanisms. Increasing the current density from 0.1 A g^{-1} to 1 A g^{-1} decreases the discharge time to 2.5 min and the potential windows of both positive and negative electrodes remain constant. A further 10-fold increase from 1 A g^{-1} to 10 A g^{-1} reduces the discharge time to 9 s. This is a very short discharge-time period and it is exclusively limited to the EDLC technology, but this newly developed LIC presents an excellent performance at this stage. Although voltage profiles are slightly distorted, the ohmic resistance of the overall system remains almost unvaried, the key reason why the LIC performs so well. Still, the potential window of the negative electrode is far too narrow compared to that of the positive electrode, indicative of the capacity limiting nature of the AC electrode. Thus, with the aim of getting the maximum capacity output from the LIC, an increase in the weight of the AC mass is needed while the mass of TiSb_2 is maintained constant.

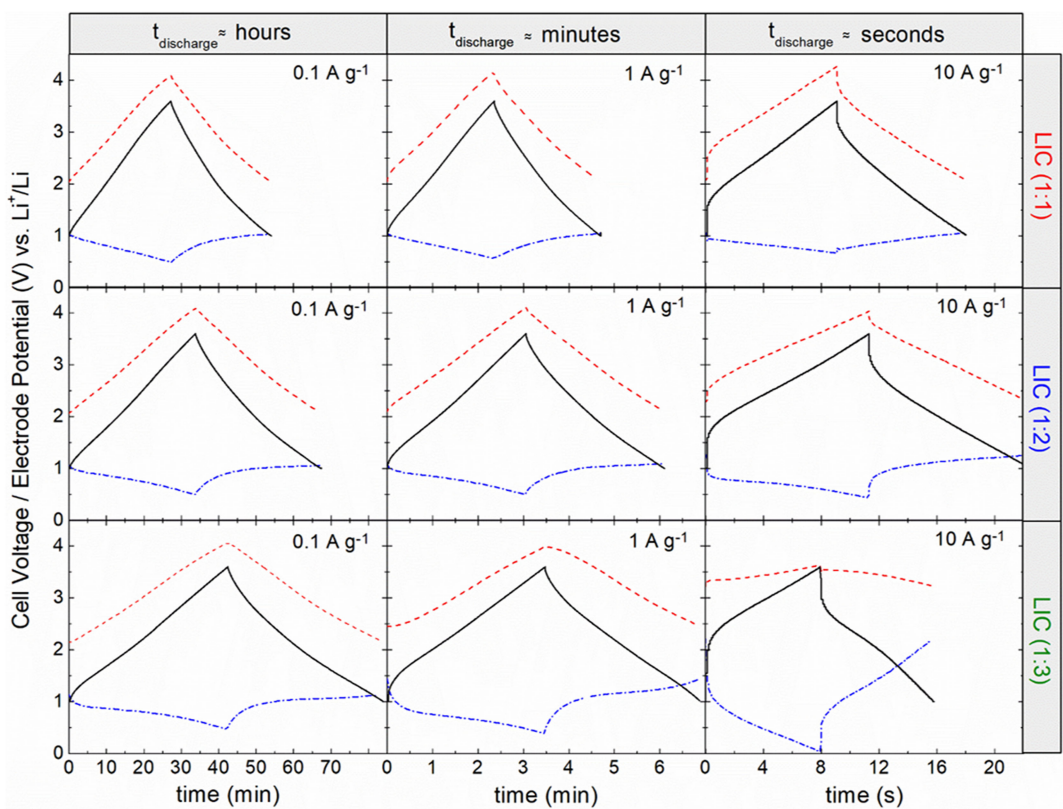


Figure 6. GA charge/discharge profiles for full LICs (black straight line), positive (AC, red dash line) and negative (TiSb_2 , blue dash-dot line) electrodes at different discharge regions.

At first sight, the new LIC (1:2), with double the AC mass relative to the negative electrode, does not infer remarkable changes in the potential window of each electrode remain similar to those measured in the initial LIC (1:1) at low current densities. However, the AC mass-increase in the positive electrode allows the negative electrode to lengthen its discharge profile and, therefore, to increase its capacity output in all the applied current density range. Thus, in LIC (1:2) a 31% specific capacitance gain (*e.g.* from 55 to 72 F g⁻¹ at 1 Ag⁻¹) is achieved through all the applied current densities owing to the mass increase of the AC electrode.

Challenging the limits, a further AC mass loading turned out in LIC (1:3). Similar to LIC (1:2), at low and medium current densities (*i.e.*, 0.1 Ag⁻¹ and 1 Ag⁻¹), a gain in the capacity output of the system is also obtained. Thus, this cell keeps the characteristic linear profile of capacitive systems while increasing the overall capacitance by 49% with respect to the initial LIC (1:1) (Figure S5). However, at high current densities (*i.e.*, 10 Ag⁻¹) the negative electrode works within a discharge time of *ca.* 8 s and a potential window that goes from 2.21 to 0.04 V. Moreover, the low minimum potential of the negative electrode can result in lithium plating and further cell short circuit, which makes LIC (1:3) unsafe in this discharge-time region. Also, due to the poor performance of the negative electrode, the operational window of the AC electrode is reduced to 0.4 V (3.6–3.2 V vs. Li⁺/Li). As a result, at high current densities the alloy limits the operation of the device, and thus, LIC (1:3) shows worsen electrochemical performance.

Both gravimetric and volumetric energy and power densities of the different LICs are reported in a Ragone plot respect the total active mass and volume of both electrodes, respectively (Figure 7a and 7b). For comparison purposes, a symmetric EDLC using the same AC and working in 1.5 M Et₄NBF₄ (acetonitrile) was built. For all the studied LICs a ~5-fold and ~4-fold increase in gravimetric and volumetric energy density terms were obtained, respectively. At low power densities, where the discharge time is about 30 min, the higher the AC loading, the higher the specific capacitance output of the system. Thus, while in LIC (1:1) system the energy density is 103 Wh kg_{AM}⁻¹, in the case of LIC (1:2) the energy reaches 129 Wh kg_{AM}⁻¹ (an increase of 30%) and 159 Wh kg_{AM}⁻¹ (an increase of 60%) in LIC (1:3). This is in good agreement with the previously observed specific capacitance gain, which translates in a higher energy density output.

At medium power densities, where the discharge time is *ca.* 3 min, LICs (1:1) and (1:2) show an excellent gravimetric energy density retention of ~88%, while LIC (1:3) presents a slightly reduced retention of ~81%. Despite this fact, the overall energy density output of LIC (1:3) is superior to LIC (1:1) and (1:2). Instead, as shown in the Ragone plot, at high power densities, when the discharge time is ~9 s, the mass overloading of the AC electrode limits the overall performance of LIC (1:3). At this point, while LIC (1:1) and LIC (1:2) systems exhibit energy density values of 52 Wh kg_{AM}⁻¹ and 66 Wh kg_{AM}⁻¹ respectively, the energy density of LIC (1:3) drops to 45 Wh kg_{AM}⁻¹, limited by the overuse of the negative electrode. The volumetric energy density values, follow the same afore-

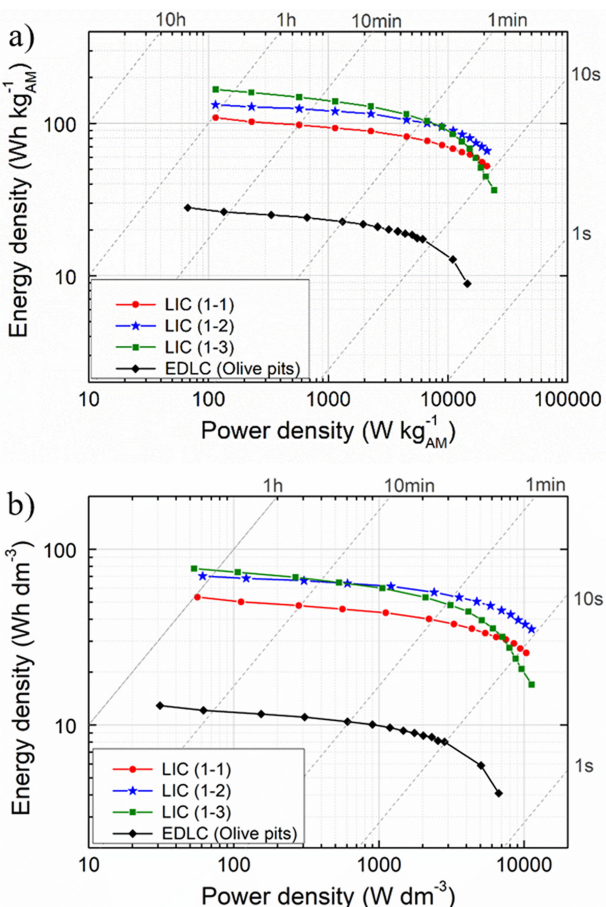


Figure 7. a) Gravimetric and b) volumetric Ragone plots comparing all studied LICs to their EDLC counterpart.

mentioned trend. Overall, owing to its excellent behavior at all power density regions in both gravimetric and volumetric terms and its safe behavior avoiding any lithium plating or electrolyte decomposition, 1:2 turned out to be the best mass ratio for this TiSb₂:AC based LIC. In fact, the energy-to-power performance of LIC (1:2) compares very well with the state of the art (see Figure S6). Furthermore, the great challenge of LICs is to keep cycle life as close as possible to that of EDLCs. In this sense, when LIC (1:2) is charged/discharged at 10 Ag⁻¹ ($t_{\text{discharge}} = 11$ s) the system shows a promising capacitance retention of 80% after 10000 cycles (Figure S7). Furthermore, if the first 50 cycles are considered as stabilizing cycles, the capacitance retention of the device rises up to 91% after 10000 cycles.

In order to gain some insight into the degradation mechanism behind this capacity fading, a post-mortem analysis was carried out after the 10000 cycles. The XRD pattern in Figure 8a shows the TiSb₂-BM material in its discharge stage after long-term cycling where two small broad maxima at 38° and 45° can be ascribed to Li₃Sb. The presence of the alloy demonstrates that the charge storage mechanism of the negative electrode is still governed by the alloying/dealloying reaction. Microstructural characterization of the electrode surface reveals some cracks due to the mechanical stress suffered

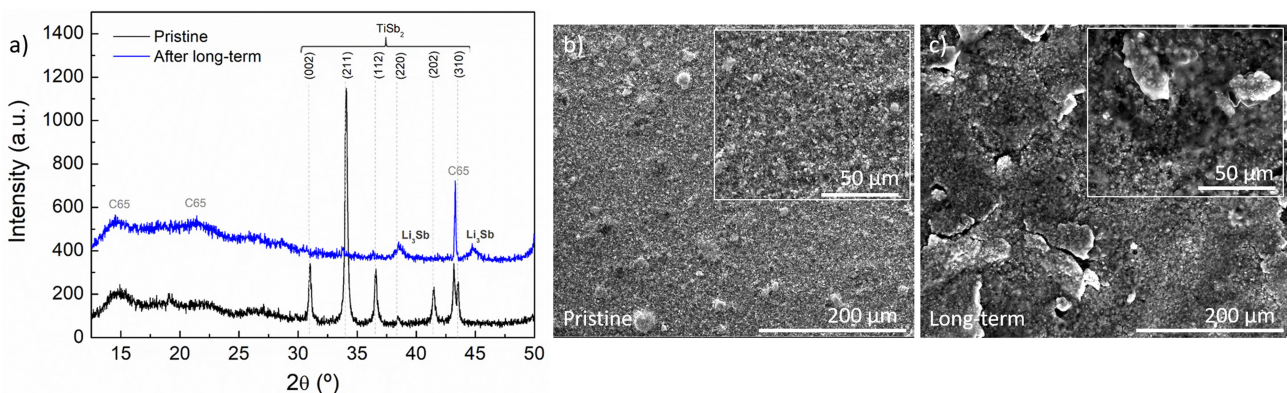


Figure 8. Post-mortem analysis of TiSb_2 negative electrode after long-term cycling in comparison with the pristine material: a) XRD patterns and SEM images: b) Pristine and c) After long-term electrodes (inset: magnifications).

upon cycling (Figure 8b and 8c). In addition, a relatively thick SEI can also be observed (inset Figure 8c). Even so, the long cyclability highlights the good mechanical properties of the studied TiSb_2 -BM negative electrode, and thus, the excellent performance of the LIC.

3. Conclusions

TiSb_2 intermetallic compound with reduced particle size was selected as a potential candidate to be used as negative electrode in hybrid supercapacitors owing to its high specific capacity values and its excellent capacity retention at high C-rates (360 mAh g^{-1} at 10 C). Thus, a novel lithium ion capacitor (LIC) using TiSb_2 alloy as the negative electrode and olive pits derived activated carbon (AC) as the positive electrode was developed. Different applications have different energy and power requirements, and we found out that there is not a suitable mass ratio to cover the overall power region providing the maximum energy at all levels. Thus, the effect of the positive-to-negative electrode mass ratio in the energy delivery and uptake was studied. Considering high power applications and also bearing in mind the importance of a safety operation, we found out LIC (1:2), *i.e.*, an AC electrode with double the mass of the TiSb_2 , to be the best performing system. This system is able to deliver $132 \text{ Wh kg}_{\text{AM}}^{-1}$ at $115 \text{ W kg}_{\text{AM}}^{-1}$ (70 Wh dm^{-3} at 61 W dm^{-3}) and $90 \text{ Wh kg}_{\text{AM}}^{-1}$ at $11053 \text{ W kg}_{\text{AM}}^{-1}$ (48 Wh dm^{-3} at 5880 W dm^{-3}). Furthermore, this device shows an outstanding capacitance retention of 80% after 10000 cycles within a discharge time of 11 s. XRD and SEM post-mortem analysis confirm the improved mechanical properties of this novel lithium ion capacitor.

Experimental Section

The TiSb_2 material was prepared by placing a stoichiometric mixture of Ti (Sigma Aldrich) and Sb (Sigma Aldrich) metals in a tubular furnace and heating them at $5 \text{ }^\circ\text{C min}^{-1}$ to $900 \text{ }^\circ\text{C}$ for 12 h under argon atmosphere (100 ml min^{-1}). After the heat treatment, the sample was first grounded in a mortar and then the particle

size was reduced by wet ball milling in a Fritsch Pulverisette 7 at 500 rpm during 2 h.

The synthesis of the AC from olive pits used in the final LIC was performed following the method previously reported by Redondo and co-authors.^[41]

X-ray diffraction (XRD) patterns for the pristine alloy and for the ball milled powder were recorded in a Bruker D8 X-ray diffractometer. Data was collected at 40 kV and 30 mA using CuK α radiation over a 2θ range between 10 – 80 $^\circ$. Scanning Electron Microscopy (SEM) images were acquired with a field emission Quanta 200 FEG microscope.

The TiSb_2 slurry was prepared by a mixture of the active material, Super P C65 (Imerys Graphite & Carbon) as conductive material and carboxymethyl cellulose (CMC) as binder in 80:10:10 mass ratio dispersed in ethanol/water solvent using IKA[®]T25 digital Ultra Turrax[®] homogenizer. The AC slurry was prepared by a mixture of active material and polyvinylidene fluoride (PVdF) as binder in a 95:5 mass ratio in N-methyl-2-pyrrolidone (NMP) followed by vigorous stirring for 1 h. Then both slurries were laminated, TiSb_2 -based one onto a copper current collector foil and AC-based slurry onto an aluminum foil. Laminates were transferred into a vacuum oven and dried at $80 \text{ }^\circ\text{C}$ under constant vacuum for 12 h before 1.13 cm^2 circular electrodes were cut out. The GA charge/discharge measurements of TiSb_2 -BM, Sb and AC electrodes were carried out in a three-electrode Swagelok[®] airtight system. When TiSb_2 and Sb were the working electrodes a second metallic Li electrode was used as counter electrode and when the AC was studied, ovesized (thicker) commercial YP-80F (Kuraray, Japan) was used as counter electrode to ensure its higher surface area not to limit the current being supplied to the working electrode. The final LIC was assembled in a three-electrode Swagelok[®] airtight system using Li metal as the reference electrode. They all use 1 M LiPF₆ in ethylene carbonate and dimethyl carbonate 1:1 (EC:DMC, v/v) as the electrolyte and a glass fiber membrane (Whatman GFB) as the separator and were assembled inside a glove box under argon atmosphere. Cyclic voltammetry (CV) and Galvanostatic (GA) charge/discharge measurements were recorded in a multichannel potentiostat (Biologic VMP3, France). The impedance measurements for TiSb_2 -BM and Sb were carried out in a two-electrode Swagelok[®] airtight system using Li metal as both counter and reference electrode and applying a low sinusoidal amplitude alternating voltage of 10 mV over zero current potential (OCP) and 50 mV at frequencies from 1 MHz to 10 mHz.

Acknowledgements

The authors would like to thank financial support by the Basque Country Government under the Elkartek 18 program (Project CICE2018). M. A. thanks the Spanish Ministry of Education, Culture and Sport (MECD) for her FPU pre-doctoral fellowship (FPU15/04876) and J.L. G.-C. acknowledges the Spanish Ministry of Economy and Competitiveness (MINECO) for the "Juan de la Cierva" fellowship (JCI-2014-20613).

Conflict of Interest

The authors declare no conflict of interest.

Keywords: TiSb₂ • activated carbon • lithium ion capacitor • supercapacitor

- [1] M. Winter, R. J. Brodd, *Chem. Rev.* **2004**, *104*, 4245–4270.
- [2] K. Naoi, *Fuel Cells*, **2010**, *10*, 825–833.
- [3] W. J. Cao, J. Shih, J. P. Zheng, T. Doung, *J. Power Sources* **2014**, *257*, 388–393.
- [4] H. Wang, C. Zhu, D. Chao, Q. Yan, H. J. Fan, *Adv. Mater.* **2017**, *29*, 1702093.
- [5] K. Naoi, S. Ishimoto, J. Miyamoto, W. Naoi, *Energy Environ. Sci.* **2012**, *5*, 9363–9373.
- [6] K. Naoi, K. Kisut, E. Iwama, S. Nakashima, Y. Sakai, Y. Orikasa, P. Leone, N. Dupré, T. Brousse, P. Rozier, W. Naoi, P. Simon, *Energy Environ. Sci.* **2016**, *9*, 2143–2151.
- [7] J. R. Miller, A. F. Burke, *The Electrochem. Soc. Interface* **2008**, *17*, 53, https://www.electrochem.org/dl/interface/spr/spr08/spr08_p53-57.pdf (accessed January 16, 2018).
- [8] Lithium Ion Capacitor – LIC | JSR Micro, Inc., <https://www.jsrmicro.com/emerging-technologies/lithium-ion-capacitor-lic> (accessed January 20, 2018).
- [9] Front runner of Lithium Ion Capacitor. JM Energy Corporation, <http://www.jmenergy.co.jp/en/> (accessed January 30, 2018).
- [10] Li-ion Capacitors – Yunasko is the developer and licensor of high power ultracapacitors, <http://yunasko.com/en/products/lithium-ion-capacitors> (accessed January 30, 2018).
- [11] S. Technologies, Ultracapacitors and supercapacitors for energy storage, <https://www.skeletontech.com> (accessed January 30, 2018).
- [12] M. T. Inc, Maxwell Technologies Delivers First Commercial Application of Lithium-Ion Capacitor Technology in China, <https://www.prnewswire.com/news-releases/maxwell-technologies-delivers-first-commercial-application-of-lithium-ion-capacitor-technology-in-china-300354618.html> (accessed January 20, 2018).
- [13] C.-L. Hsieh, D.-S. Tsai, W.-W. Chiang, Y.-H. Liu, *Electrochim. Acta* **2016**, *209*, 332–340.
- [14] B. Babu, P. G. Lashmi, M. M. Shajumon, *Electrochim. Acta* **2016**, *211*, 289–296.
- [15] S. Jayaraman, A. Jain, M. Ulaganathan, E. Edison, M. P. Srinivasan, R. Balasubramanian, V. Aravindan, S. Madhavi, *Chem. Eng. J.* **2017**, *316*, 506–513.
- [16] G. Wang, C. Lu, X. Zhang, B. Wan, H. Liu, M. Xia, H. Gou, G. Xin, J. Lian, Y. Zhang, *Nano Energy* **2017**, *36*, 46–57.
- [17] P. Sennu, V. Aravindan, Y.-S. Lee, *Chem. Eng. J.* **2017**, *324*, 26–34.
- [18] E. Lim, W.-G. Lim, C. Jo, J. Chun, M.-H. Kim, K. C. Roh, J. Lee, *J. Mater. Chem. A* **2017**, *5*, 20969–20977.
- [19] J. Ajuria, E. Redondo, M. Arnaiz, R. Mysyk, T. Rojo, E. Goikolea, *J. Power Sources* **2017**, *359*, 17–26.
- [20] C.-M. Lai, T.-L. Kao, H.-Y. Tuan, *J. Power Sources* **2018**, *379*, 261–269.
- [21] X. Xu, F. Niu, D. Zhang, C. Chu, C. Wang, J. Yang, Y. Qian, *J. Power Sources* **2018**, *384*, 240–248.
- [22] X. Zhu, D. Sun, B. Luo, Y. Hu, L. Wang, *Electrochim. Acta* **2018**, *284*, 30–37.
- [23] Q. Lu, B. Lu, M. Chen, X. Wang, T. Xing, M. Liu, X. Wang, *J. Power Sources* **2018**, *398*, 128–136.
- [24] M. Arnaiz, C. Botas, D. Carriazo, R. Mysyk, F. Mijangos, T. Rojo, J. Ajuria, E. Goikolea, *Electrochim. Acta* **2018**, *284*, 542–550.
- [25] V. Aravindan, J. Gnanaraj, Y.-S. Lee, S. Madhavi, *Chem. Rev.* **2014**, *114*, 11619–11635.
- [26] D. Cericola, R. Kötz, *Electrochim. Acta* **2012**, *72*, 1–17.
- [27] C.-M. Park, J.-H. Kim, H. Kim, H.-J. Sohn, *Chem. Soc. Rev.* **2010**, *39*, 3115–3141.
- [28] C. Wang, Y. Li, Y.-S. Chui, Q.-H. Wu, X. Chen, W. Zhang, *Nanoscale* **2013**, *5*, 10599–10604.
- [29] H. Shang, Z. Zuo, L. Yu, F. Wang, F. He, Y. Li, *Adv. Mater.* **2018**, *30*, 1801459.
- [30] H. Lv, S. Qiu, G. Lu, Y. Fu, X. Li, C. Hu, J. Liu, *Electrochim. Acta* **2018**, *151*, 214–221.
- [31] Z. Yi, Q. Han, P. Zan, Y. Wu, Y. Cheng, L. Wang, *J. Power Sources* **2016**, *331*, 16–21.
- [32] S. Goriparti, E. Miele, F. De Angelis, E. Di Fabrizio, R. Proietti Zaccaria, C. Capiglia, *J. Power Sources* **2014**, *257*, 421–443.
- [33] U. Kasavajjula, C. Wang, A. J. Appleby, *J. Power Sources* **2007**, *163*, 1003–1039.
- [34] W. Luo, J.-J. Gaumet, L.-Q. Mai, *Rare Met.* **2017**, *36*, 321–338.
- [35] P. Nithyadhariseni, M. V. Reddy, B. Nalini, M. Kalpana, B. V. R. Chowdari, *Electrochim. Acta* **2015**, *161*, 261–268.
- [36] C. Villevieille, C. M. Ionica-Bousquet, B. Fraisse, D. Zitoun, M. Womes, J. C. Jumas, L. Monconduit, *Solid State Ionics* **2011**, *192*, 351–355.
- [37] J. L. Gómez-Cámer, C. Villevieille, P. Novák, *J. Mater. Chem. A* **2013**, *1*, 13011–13016.
- [38] J. L. Gómez-Cámer, P. Novák, *J. Power Sources* **2015**, *273*, 174–179.
- [39] P. Scherrer, Nachrichten von der Gesellschaft der Wissenschaften zu Göttingen, *Mathematisch-Physikalische Klasse* **1918**, 98–100.
- [40] S. Dsoke, B. Fuchs, E. Gucciardi, M. Wohlfahrt-Mehrens, *J. Power Sources* **2015**, *282*, 385–393.
- [41] E. Redondo, J. Carretero-González, E. Goikolea, J. Ségalini, R. Mysyk, *Electrochim. Acta* **2015**, *160*, 178–184.

Manuscript received: October 5, 2018

Accepted manuscript online: October 16, 2018

Version of record online: November 14, 2018